Optics Letters

Realization of broadband cross-polarization conversion in transmission mode in the terahertz region using a single-layer metasurface

Wenwei Liu,[1] Shuqi Chen,[1,*] Zhancheng Li,[1] Hua Cheng,[1] Ping Yu,[1] Jianxiong Li,[1] and Jianguo Tian[1,2]

[1]The Key Laboratory of Weak Light Nonlinear Photonics, Ministry of Education, School of Physics and Teda Applied Physics Institute, Nankai University, Tianjin 300071, China
[2]e-mail: jjtian@nankai.edu.cn
*Corresponding author: schen@nankai.edu.cn

Received 7 April 2015; revised 10 June 2015; accepted 10 June 2015; posted 11 June 2015 (Doc. ID 237637); published 30 June 2015

We present the design specifications and in-depth analysis of a terahertz (THz) broadband cross-polarization converter composed of a single-layer metasurface. This device can convert linearly polarized light into its cross-polarization in transmission mode. Different from other polarization conversion devices, this effect results from the suppression and enhancement for different electric components. The broadband characteristic is also achieved by specific partial symmetries designed in the structure. The proposed polarization converter can aid in the development of novel plasmonic polarization devices, and can help to overcome certain limitations of the customary designs that have been proposed thus far.

OCIS codes: (160.3918) Metamaterials; (240.6680) Surface plasmons; (040.2235) Far infrared or terahertz.

http://dx.doi.org/10.1364/OL.40.003185

Since the development of efficient terahertz (THz) sources and sensitive detectors in recent years, THz technology has garnered tremendous attention in the scientific community. Today, unprecedented THz applications have been studied widely in relation to security screening, communications, sensing, etc. [1]. However, further applications are restricted by the lack of effective THz manipulation devices—such as polarization rotators, lenses, and phase modulators [2,3]. The polarization state of THz waves is conventionally controlled by using dichroic crystals or birefringent materials [4,5], which leads to a very narrow response waveband because of the crystal-based properties; this also results in difficulties in THz system miniaturization and integration.

Recently, polarization modulation using plasmonic metasurfaces or metamaterials has made considerable developments in the form of artificial planar and three-dimensional chiral structures [6,7], spiral bull's-eye structures [8], planar nonchiral metamaterials [9], and multi-layer structures [10,11]. For example, Li *et al.* proposed an *L*-shaped nanostructure to manipulate the polarization state of the incident light [12]. However, mechanisms of this kind of design are based on charge transfer in the corner of the structure, which limits the potential for polarization conversion, and can rotate only the polarization angle of incidence by no more than 45°.

More recently, many multi-layer structures have been proposed to realize high-efficiency polarization manipulation. Most of these plasmonic polarization modulators operate in reflection mode [13–15]. This is caused mainly by the effective interactions among the electromagnetic waves and the modulators that occur in reflection mode. However, polarization modulation in transmission mode is preferable because of its intrinsic convenience for experimental and commercial utilization.

One way to achieve polarization conversion in transmission mode is by placing the nanostructure between two orthogonally oriented gratings [16]. However, such polarization rotators are multi-layer structures, which complicates the fabrication process and frustrates efforts toward the nanoscale integration of such devices. Another method for achieving a large polarization rotation angle in transmission mode is combining the surface plasmon polaritons (SPPs) with localized surface plasmon (LSP) resonances [17]. However, this method leads to an inherently narrow band because the combination of the two effects requires stringent conditions that are not satisfied easily under certain superposition conditions. Thus, a broadband single-layer cross-polarization converter in transmission mode is a fascinating prospect, and has not been realized in the previous works.

In this Letter, we present the design specifications and in-depth analysis of a THz broadband cross-polarization converter in transmission mode composed of a single-layer metasurface. We show that if the LSP resonances of the metasurface can be

stimulated well and form an electric-field phase change of π in the horizontal direction (i.e., parallel to the incident polarization) and a phase change of 0 in the orthogonal direction, a nearly 90° rotation would be realized with one single layer. Moreover, the partial symmetry of the structure is responsible for the broadband THz cross-polarization behavior. The proposed mechanisms may have a profound impact on polarization conversion devices, as a new platform for integrated subwavelength systems.

A schematic diagram of the designed cross-polarization converter is illustrated in Fig. 1(a). The x-polarized transverse electromagnetic (TEM) wave irradiates the subwavelength structure, and y-polarized emergent light is observed. The proposed converter is composed of two rotationally symmetric "F" shapes with the central line connected. The unit cell of the structure is shown in Fig. 1(b), in which the thickness of the thin metallic film is 200 nm.

The structure is designed based on the following principles. On the one hand, the overall asymmetry of the structure is required to achieve polarization manipulation [18]. More specifically, the symmetry broken structure interacts with the incident light leading to charge transfer, which generates an electric component of light perpendicular to the original one. On the other hand, the partial symmetry of the structure is also necessary to improve the incident frequency tolerance, which will be stated in detail in the following discussion. The finite element method (FEM)-based software COMSOL Multiphysics [19] was used to design and optimize the polarization rotator. In the simulation, the gold was characterized with a conductivity $\sigma_{dc} = \varepsilon_0\omega_p^2\tau$, where $\omega_p = 2175$ THz is the plasma frequency, and $\tau = 24.5$ fs is the scattering relaxation time [20]. Periodic boundary conditions were imposed in the x- and y-directions to characterize the periodic structure, and the scattering boundary condition was set as a source. The polarization of the incident light is x-polarized in all our simulations.

The transmitted light is basically elliptically polarized in the waveband under consideration, and can be described by the following equation:

$$\frac{x^2}{E_x^2} + \frac{y^2}{E_y^2} - 2\frac{\cos\delta}{E_x E_y}xy = \sin^2\delta, \tag{1}$$

where $\delta = \varphi_y - \varphi_x$ is the phase difference of the transmitted electric field components E_y and E_x. As depicted below, the energy corresponding to the main axis of the elliptical light dominates the total transmitted light. We use the angle between the main axis of the transmitted light and the incident polarization direction (i.e., along the x axis) to characterize the polarization rotation angle θ, as shown in Fig. 2. In the range of 0.87–1.47 THz, θ is larger than 75°, and reaches its peaks of 88° and 87° for 0.92 and 1.38 THz incidence, respectively. For 1.38 THz incident light, the rotary power ρ (which is defined by the rotation angle per unit length) reaches 4.35×10^5 degree/mm, which is several orders of magnitude larger than that of natural birefringent crystal [21]. Furthermore, the response bandwidth is much larger than that of the combined SPP and LSP resonances [17], which is hard to achieve owing to the rigid coupling conditions. This remarkable characteristic can also be demonstrated by the polarization conversion rate (PCR), which is defined as

$$\mathrm{PCR} = t_{yx}^2/(t_{yx}^2 + t_{xx}^2), \tag{2}$$

where t_{ij} denotes i-polarized electric transmission from j-polarized incident light. It is clear that in the range of 0.91–1.45 THz, over 90% of the energy of the transmitted light belongs to the cross-polarization component.

To better illustrate the quality of the emergent light, a simulated polarizer is used to detect the transmitted light. As the polarizer rotates from 0 to 2π, the normalized transmitted energy varies from 0 to 1. The simulation is shown in Fig. 3(a), in which the red line represents the ideal results with only a y-polarized source and a polarizer, whereas the blue stars indicate the results from our polarization conversion film mimicking the y-polarized source; the frequency of the incident light is 1.38 THz in the x-direction. The two sets of results are close to each other, which demonstrates that we successfully obtained high-quality, nearly orthogonally polarized emergent light. The electric transmittance for the x- and y-polarized components is also shown in Fig. 3(b). The transmitted electric field in the x-direction is suppressed as t_{xx} approaches zero. If the incident light is y-polarized, the effect of polarization conversion

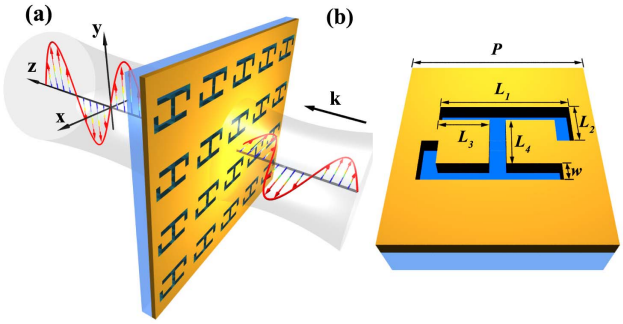

Fig. 1. (a) Schematic diagram of the single-layer linear polarization converter, where yellow stands for gold and blue indicates the substrate. An x-polarized incident beam is converted to a y-polarized beam, and the direction of the wave vector is along the $+z$ axis. (b) Unit cell of the structure, which is centrosymmetric about the z axis. Geometrical parameters include $L_1 = 130$ μm, $L_2 = 40$ μm, $L_3 = 50$ μm, $L_4 = 48$ μm, $P = 190$ μm, and $w = 16$ μm.

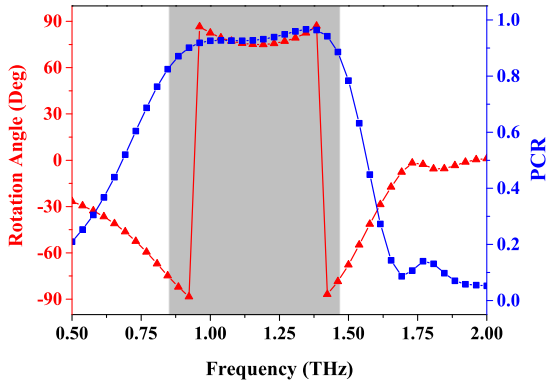

Fig. 2. Dependence of the polarization rotation angle θ (red triangle line) and PCR (blue square line) on the THz waveband. The gray zone indicates the bandwidth corresponding to $\theta > 75°$.

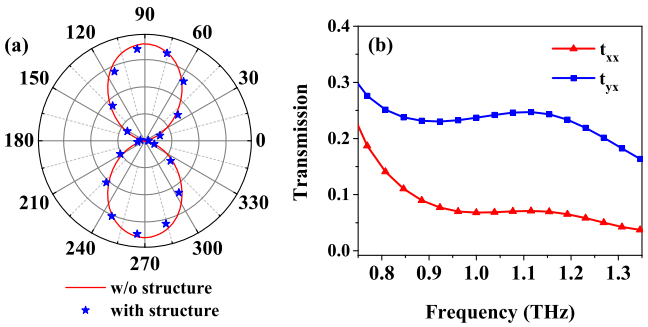

Fig. 3. (a) Comparison of transmission for different analyzer angles with 1.38 THz incident light. The red line indicates the ideal result for y-polarized incidence without the structure, whereas the blue stars represent the computed transmission for x-polarized incident light with the structure. (b) Calculated transmittance for x and y electric components.

is very weak and most of the transmitted light is also y-polarized. In the simulation, the intensity of the transmitted electric field was integrated at a distance of 200 μm away from the metasurface, which was normalized by the incident one.

To gain insight into the nature of the polarization conversion mechanism, we simulate the electric field distributions for E_x and E_y on the bottom surface of the gold layer for 1.00 THz incident light, as shown in Figs. 4(a) and 4(b). The aggregation of the electric field is mainly dependent on the shape of the holes in the metallic film, which evidences the stimulation of LSPs [22]. Here, the E_x component in zone (1) and zone (2) possesses a phase difference of π, thus leading to reciprocal inhibition. With careful designs, the summation of E_x on the top surface of the structure (one unit cell) can approach zero, which is vital for cross-polarization conversion with a single-layer metasurface. By way of contrast, the E_y distribution maintains the same phase throughout the surface, as shown in zone

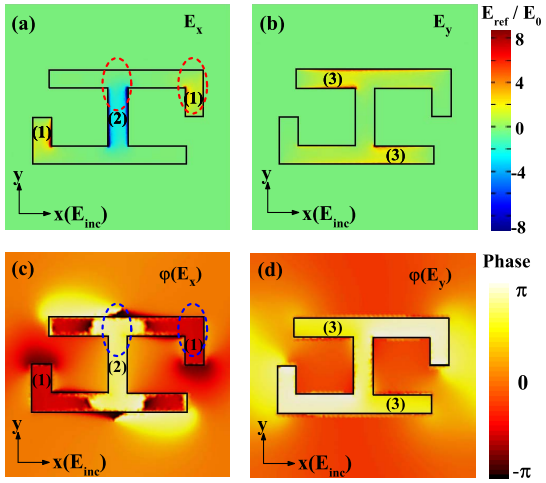

Fig. 4. Near-field (a) E_x and (b) E_y distributions for 1.00 THz incident light on the bottom surface of the metasurface. The red dashed circles indicate suppression areas resulting from the partial symmetric structure. Zones (1)–(3) indicate excited LSP resonance areas with different distributions of electric intensity and phase. (c) and (d) are the phase distributions of E_x and E_y on the bottom surface for 1.00 THz incidence.

(3), which results in mutual promotion. It is worth mentioning that the electric field distribution interpreted above remains the same throughout the entire waveband in question. On the one hand, to generate ideal suppression for E_x, a relatively symmetric structure leading to the same electric intensity and an electric phase difference of π is required. As shown in Fig. 4(a) [red dashed circle], the two regions with similar slot shapes stimulate striking resemblance to LSPs with a phase difference of π, which tremendously improves the incident frequency tolerance. On the other hand, the overall asymmetry is a precondition for the polarization converter, as stated before. Hence, a broadband polarization rotator is achieved with one gold layer. This is a different way of broadband realization from the phase compensation [23]. To get insight into the phase difference of the excited LSPs, we plotted the phase distribution for E_x and E_y on the bottom metasurface for 1.00 THz incidence, as shown in Figs. 4(c) and 4(d). A phase difference of π between zones (1) and (2) in Fig. 4(c) is apparent. The enhancement between two zones (3) in Fig. 4(d) can be achieved. The phase difference in a whole harmonic cycle is always unchanged.

The partial symmetry of the structure is related mainly with the geometrical parameter L_2, which strongly affects the interference of the electric field between zones (1) and (2). As shown in Fig. 5(a), the PCR has a red shift with the increasing of L_2. The peak value and width of the PCR spectrum is optimal when $L_2 = 40$ μm. Comparing with other geometrical parameters, the thickness of the gold layer almost does not affect the PCR, as shown in Fig. 5(b). This mainly results from the shape-dependence of LSP excitation and the high conductivity of gold in this waveband. To demonstrate the broadband effect arising from the partial symmetry of the structure, we give the near-field distributions for E_x and E_y with 1.15 THz incidence in the insets of Figs. 5(a) and 5(b), which are similar to the results with 1.00 THz incidence in Figs. 4(a) and 4(b).

Our proposed structure is not unique among single-layer LSP resonance-based cross-polarization conversion devices. We test another h-shaped metallic slot structure to support our theory, which is illustrated in the insets of Fig. 5(c).

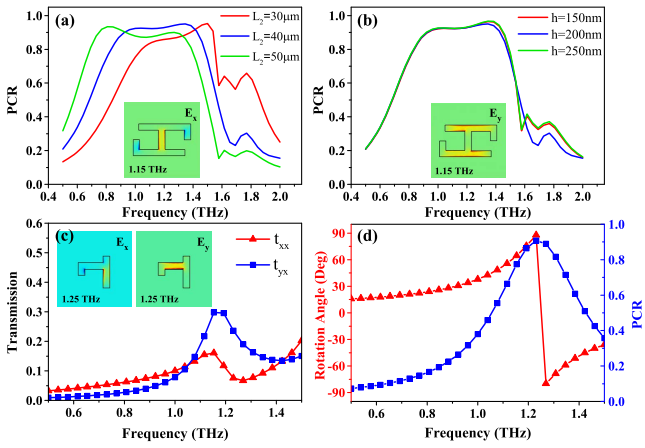

Fig. 5. PCR for different length of (a) L_2 and (b) h. Insets: near-field E_x and E_y distribution with 1.15 THz incident light. (c) t_{xx} and t_{yx} for an h-shaped structure. Inset: near-field E_x and E_y distribution with 1.25 THz incident light. (d) Calculated polarization rotation angle θ and PCR for the h-shaped structure.

Similar to the LSP resonances in Figs. 4(a) and 4(b), the electric field distributions also reveal a strong localized resonance with a phase difference of π and 0 at the cross-polarization conversion frequency 1.25 THz, which proves that the electric suppression in x-direction and enhancement in y-direction are realized simultaneously. The electric transmission spectra, polarization rotation angle, and PCR are also shown in Figs. 5(c) and 5(d). The capability for polarization conversion of the metallic slot film decreases rapidly when the incident frequency departs from 1.25 THz. This is mainly because of highly asymmetric parts of the structure that correspond to zones of phase difference of π; such parts extraordinarily affect the intensity and phase of the LSP resonances, which is in sharp contrast to the electric distributions in Fig. 4. For experimental characterization, the proposed single-layer metasurface can be fabricated easily through sputtering deposition, electron-beam lithography, and reactive-ion etching techniques. The sample can be characterized using a fiber-coupled photoconductive dipole antenna based terahertz time-domain spectrometer (THz-TDS) incorporating two polarizers, which can be configured to operate in transmission.

In conclusion, we have proposed a broadband cross-polarization rotator composed of a single metallic slot layer in the THz region in transmission mode. This effect results from the superposition of electromagnetic waves generated by LSP resonances, which is different from previous studies on polarization conversion. With suitable design parameters, an electric phase difference of π in one direction and zero in the other direction, are achieved simultaneously. The proposed polarization rotator functions very well in a broadband region owing to the partial symmetry of the structure. Moreover, any structure can accomplish similar effects, provided that the stimulation conditions are satisfied. This result offers helpful insight on cross-polarization conversion, and furthermore suggests intriguing possibilities regarding the development of planar vector beam devices, wavefront modulation devices in the THz domain, as well as other regions of the electromagnetic spectrum.

Funding. Chinese National Key Basic Research Special Fund (2011CB922003); International Science & Technology Cooperation Program of China (2013DFA51430); National Basic Research Program (973 Program) of China (2012CB921900); Natural Science Foundation of China (NSFC) (11304163, 61378006); Natural Science Foundation of Tianjin (13JCQNJC01900); Program for New Century Excellent Talents in University (NCET-13-0294); 111 project (B07013).

REFERENCES

1. T. Kleine-Ostmann and T. Nagatsuma, J. Infrared Milli. Terahz. Waves **32**, 143 (2011).
2. S. C. Jiang, X. Xiong, Y. S. Hu, Y. H. Hu, G. B. Ma, R. W. Peng, and M. Wang, Phys. Rev. X **4**, 021026 (2014).
3. B. Gholipour, J. Zhang, K. F. MacDonald, D. W. Hewak, and N. I. Zheludev, Adv. Mater. **25**, 3050 (2013).
4. D. Grischkowsky, Appl. Phys. Lett. **57**, 1055 (1990).
5. F. Rutz, T. Hasek, M. Koch, H. Richter, and U. Ewert, Appl. Phys. Lett. **89**, 221911 (2006).
6. B. Bai, Y. Svirko, J. Turunen, and T. Vallius, Phys. Rev. A **76**, 023811 (2007).
7. J. K. Gansel, M. Thiel, M. S. Rill, M. Decker, K. Bade, V. Saile, and M. Wegener, Science **325**, 1513 (2009).
8. P. Genevet, J. Lin, M. A. Kats, and F. Capasso, Nat. Commun. **3**, 1278 (2012).
9. E. Plum, X. X. Liu, V. A. Fedotov, Y. Chen, D. P. Tsai, and N. I. Zheludev, Phys. Rev. Lett. **102**, 113902 (2009).
10. R. H. Fan, Y. Zhou, X. P. Ren, R. W. Peng, S. C. Jiang, D. H. Xu, and M. Wang, Adv. Mater. **27**, 1201 (2015).
11. C. P. Huang, Q. J. Wang, X. G. Yin, Y. Zhang, J. Q. Li, and Y. Y. Zhu, Adv. Opt. Mater. **2**, 723 (2014).
12. T. Li, S. M. Wang, J. X. Cao, H. Liu, and S. N. Zhu, Appl. Phys. Lett. **97**, 261113 (2010).
13. A. Pors, M. G. Nielsen, G. D. Valle, M. Willatzen, O. Albrektsen, and S. I. Bozhevolnyi, Opt. Lett. **36**, 1626 (2011).
14. Q. Lévesque, M. Makhsiyan, P. Bouchon, F. Pardo, J. Jaeck, N. Bardou, and J. L. Pelouard, Appl. Phys. Lett. **104**, 111105 (2014).
15. H. Cheng, S. Chen, P. Yu, X. Duan, B. Xie, and J. Tian, Appl. Phys. Lett. **103**, 203112 (2013).
16. N. K. Grady, J. E. Heyes, D. R. Chowdhury, Y. Zeng, M. T. Reiten, A. K. Azad, and H.-T. Chen, Science **340**, 1304 (2013).
17. S. Wu, Z. Zhang, Y. Zhang, K. Zhang, L. Zhou, X. Zhang, and Y. Zhu, Phys. Rev. Lett. **110**, 207401 (2013).
18. P. Ginzburg, F. J. Rodríguez-Fortuño, A. Martínez, and A. V. Zayats, Nano Lett. **12**, 6309 (2012).
19. COMSOL Multiphysics User's Guide, Version 4.3.1.115 (Comsol AB, Burlington, MA, 2012).
20. A. Thoman, A. Kern, H. Helm, and M. Walther, Phys. Rev. B **77**, 195405 (2008).
21. A. Yariv and P. Yeh, *Optical Waves in Crystals* (Wiley, 1984).
22. M. Schwind, B. Kasemo, and I. Zorić, Nano Lett. **13**, 1743 (2013).
23. F. Aieta, M. A. Kats, P. Genevet, and F. Capasso, Science **347**, 1342 (2015).